Deformation and breakup of high-viscosity droplets with symmetric microfluidic cross flows

Thomas Cubaud*
Department of Mechanical Engineering, Stony Brook University, Stony Brook, New York 11794, USA
(Received 15 April 2009; revised manuscript received 23 July 2009; published 19 August 2009)

The dynamic response of highly viscous droplets to a sharp increase in the surrounding liquid velocity is experimentally investigated in a square microchannel junction. The local injection of the continuous phase from symmetric side channels onto a train of droplets produces a large velocity contrast between the front and the rear of droplets, yielding a broad range of time-dependent deformation and breakup. In particular, due to microscale confinement, the system displays a nonlinear behavior with the initial droplet size. Deformations, relaxation times, and fragmentation processes are examined as a function of flow parameters and fluids properties with emphasis on the formation of slender viscous structures such as spoon-shaped droplets, i.e., asymmetrical droplets.

DOI: 10.1103/PhysRevE.80.026307 PACS number(s): 47.55.df, 47.15.G−, 47.20.Ma, 47.61.Jd

The shape of high-viscosity droplets translating in a straight square microchannel can be controlled using symmetric cross flows. The dynamics of droplets in viscous environments plays a critical role in producing and structuring immiscible dispersions. Considerable progress has been made in understanding the deformation, breakup, and coalescence of droplets in both simple shear and extensional flows using four-roll mill apparatuses [1–3]. For instance, the more viscous fluid governs the droplet deformation rate, and the breakup of high-viscosity ratio droplets is inhibited in simple shear flows [4]. The behavior of droplets in confined pressurized systems, however, can considerably differ from unbounded flows due to the effect of nearby boundaries. In particular, the translation of lubricated drops having a size comparable to that of the confining system is important for multiphase flows in porous media [5,6] and microfluidic networks [7,8]. A variety of microchannel designs have been investigated to generate arrays of identical droplets [9–11]. Techniques for handling pressurized trains of low-viscosity droplets in small passages rely mainly on duct geometries and include breakup at channel junctions [12–15] and constrictions [16,17], merging [18,19], and storing [20]. This area of research is motivated in part by the substantial range of applications of microfluidic drops as microreactors for sequestrating reactive materials. Soft material synthesis and diagnostic in confined microsystems, however, require the development of methods for manipulating high-viscosity droplets. A promising means for adjusting droplet specific area and residence time in microfluidic devices consists in forming threads made of highly viscous liquids ensheathed in less viscous liquids [11].

Here, we examine the deformation and breakup of high-viscosity droplets resulting from a large difference in velocities between the rear and the front of translating droplets at a channel junction. The geometry consists of two-step hydrodynamic focusing junctions with square microchannels and is characterized by a single length scale h (Fig. 1). Droplets are generated at the first focusing section by injecting a silicone oil (liquid $L1$), having a viscosity η_1, into the central channel at a flow rate Q_1, and by injecting a continuous phase of ethanol (liquid $L2$), having a viscosity η_2, into the side channel at a total flow rate Q_2. Droplets are manipulated at the second section with an additional symmetrical side injection of $L2$ at a total flow rate Q_3. Experiments are conducted for five droplet viscosities $\eta_1=19$, 48, 97, 193, and 486 cP and $\eta_2=1.14$ cP using transparent silicon and glass microchannels of height $h=100$ or 250 μm. The interfacial tension γ_{12} for each fluid pair is measured using the double capillary rise technique [21] and ranges from 0.3 to 1.5 mN m^{-1}.

In the first junction, droplets are continuously produced into the main square microchannel in the dripping regime [22], i.e., droplets form in the focusing section [11]. In the asymptotic regime associated with large viscosity contrasts, $\chi=\eta_1/\eta_2\geq 15$, we previously found that dripping occurs when each injection capillary number, $\mathrm{Ca}_i=\eta_i Q_i/(\gamma_{12}h^2)$ associated with liquid Li and i is an integer index, is lower than the critical capillary number $\mathrm{Ca}_c\approx 10^{-1}$ at which viscous and capillary stresses balance [11]. The length d_0 of small elongated droplets, i.e., $d_0/h\leq 2.5$, scales as $d_0/h\approx a(\alpha_2\mathrm{Ca}_2)^b$, where the constants are $a=0.5$ and $b=-0.17$, and the continuous phase homogeneous volume fraction is $\alpha_2=Q_2/(Q_1+Q_2)$. This production method allows for a precise control of the initial droplet size and distribution prior to cross-flow manipulations. In the second junction, significant droplet deformations occur when $Q_3\gg Q_1+Q_2$. Over the range of parameters investigated, three typical regimes are observed: "relaxing" [Fig. 1(a)], where droplets experience a modest deformation and recoil in the outlet channel, "convective breakup" [Fig. 1(b)], where droplets experience a large deformation that evolves into breakup as droplets are advected further downstream, and "absolute breakup" [Fig. 1(c)], where droplets fragment in the focusing section.

To quantify droplet deformation at the second junction, we define the effective side-flow volume fraction $\alpha_3=Q_3/(Q_d+Q_3)$, where Q_d is the droplet volume flow rate. Since droplets initially flow at relatively low capillary number and occupy most of the channel cross section, their initial velocity V_0 is comparable to the homogeneous two-phase superficial velocity $J_0=(Q_1+Q_2)/h^2$, i.e., $V_0/J_0\approx 1$. Therefore, at the junction $Q_d\approx Q_1+Q_2$, which yields $\alpha_3=Q_3/$

*Author to whom correspondence should be addressed; thomas.cubaud@stonybrook.edu

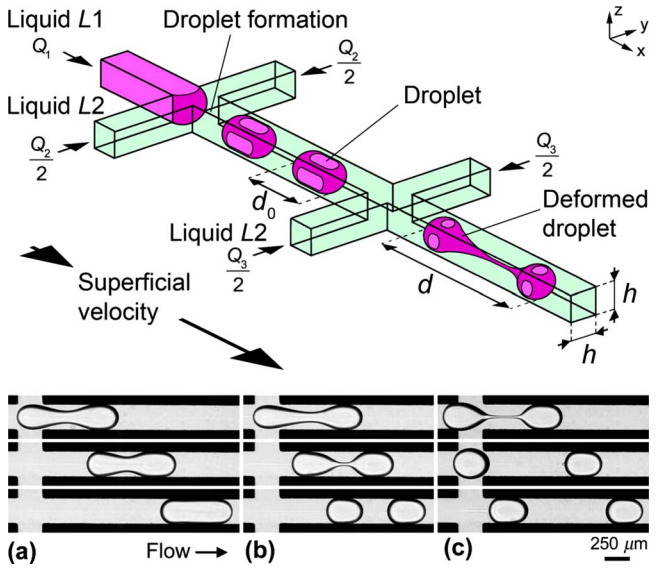

FIG. 1. (Color online) High-viscosity droplets in microfluidic cross flows. Top: two-step hydrodynamic sections in series. Bottom: experimental time series of typical regimes, $\chi=\eta_1/\eta_2=85$, flow rates in μl/min, time intervals in ms. (a) Relaxing ($Q_1=1$, $Q_2=2$, $Q_3=10$, and $\Delta t=160$), (b) convective breakup ($Q_1=1$, $Q_2=2$, $Q_3=15$, and $\Delta t=64$), and (c) absolute breakup ($Q_1=0.5$, $Q_2=1$, $Q_3=10$, and $\Delta t=26$).

$(Q_1+Q_2+Q_3)$. By analogy with droplet formation from a continuous stream of $L1$, we use $\alpha_3\mathrm{Ca}_3$ to locate deformation regimes on a phase diagram for different initial droplet size d_0/h (Fig. 2). For small droplets, the deformation is limited by the caps formed by the droplet ends having a typical curvature $\kappa\sim 2/h$. Given the small interfacial area available, altering the morphology of such droplets requires increasing κ, which is achieved with large side-flow capillary number Ca_3. On the contrary, larger droplets can be readily deformed

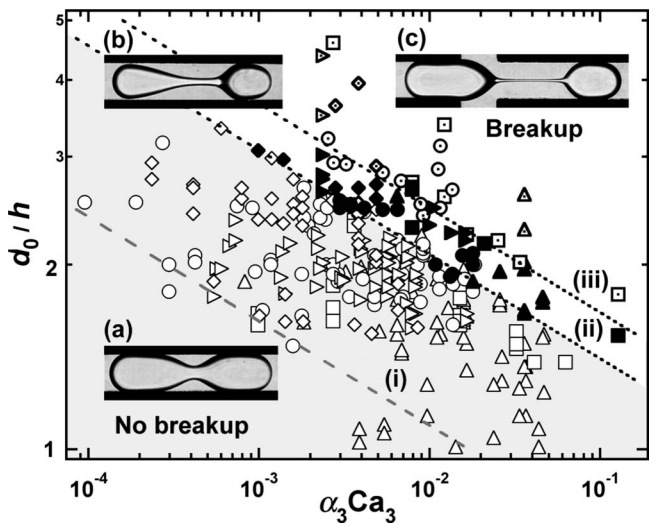

FIG. 2. Phase diagram of droplet deformation. Viscosity contrast: $\chi=17$ (△), 42 (□), 85 (○), 169 (▷), and 426 (◇). (a) Relaxing deformation (open symbols). (b) Convective breakup (filled symbols). (c) Absolute breakup (dotted symbols). Dashed lines: $d_0/h=a(\alpha_3\mathrm{Ca}_3)^{-0.17}$ with $a=0.5$ (i), 0.95 (ii), and 1.13 (iii).

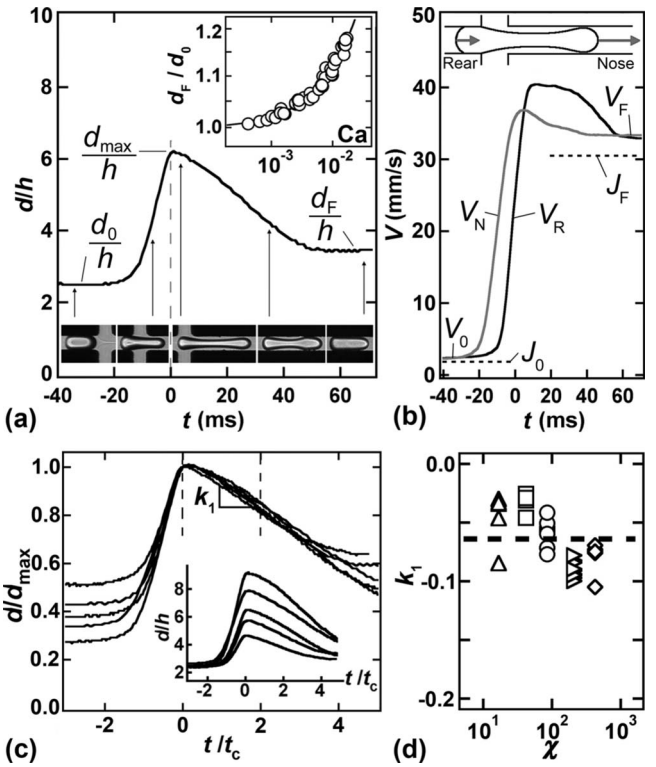

FIG. 3. Dynamics of relaxed deformation. (a) Temporal evolution of a droplet length d/h during relaxing deformation where d_0 is the initial length, $d_{\max}$ is the maximal elongation, and d_F is the final length. Inset: evolution of d_F/d_0 vs capillary number Ca. (b) Corresponding temporal evolution of droplet nose velocity V_N and rear velocity V_R during deformation where J_0 and J_F are the initial and final homogeneous superficial velocities. (c) Evolution of droplet lengths d scaled by maximal elongation $d_{\max}$ vs time t scaled by viscous-capillary time t_c. Inset: temporal evolution of droplet lengths d/h for different elongation $d_{\max}/h$. (d) Evolution of k_1 vs viscosity ratio χ. Dashed line: $k_1=-0.068$.

while preserving the initial cap curvature κ. The transition curves between regimes show the critical initial droplet size for convective or absolute breakup. These curves are fitted using the same functional form: $a(\alpha_3\mathrm{Ca}_3)^b$ with $a=0.95$ for convective breakup and $a=1.13$ for absolute breakup, and $b=-0.17$. The exponent b is similar to the one found during droplet formation from a continuous high-viscosity stream.

The evolution of the droplet length $d(x,t)$ is calculated from high-speed movies during the relaxing regime [Fig. 3(a)]. First, a time-space diagram is constructed from a line plotted along the axis of the main channel. Second, the positions of the droplet nose $x_N(t)$ and rear $x_R(t)$ are extracted from the diagram. This method allows for determining $d=x_N-x_R$ as well as the nose velocity $V_N=dx_N/dt$ and rear velocity $V_R=dx_R/dt$ during the deformation process [Fig. 3(b)]. The maximum elongation $d_{\max}$ is observed when the rear of the droplet enters the junction. Therefore, to compare experiments, we define $x=0$ at the left edge of the cross and time is set to $t=0$ when $x_R=0$. The final relaxed droplet size d_F is slightly larger than d_0 due to the large increase of the continuous phase capillary number $\mathrm{Ca}=(\eta_2\Sigma Q_i)/(h^2\gamma_{12})$ in the straight channel after the junction. Indeed, as the thick-

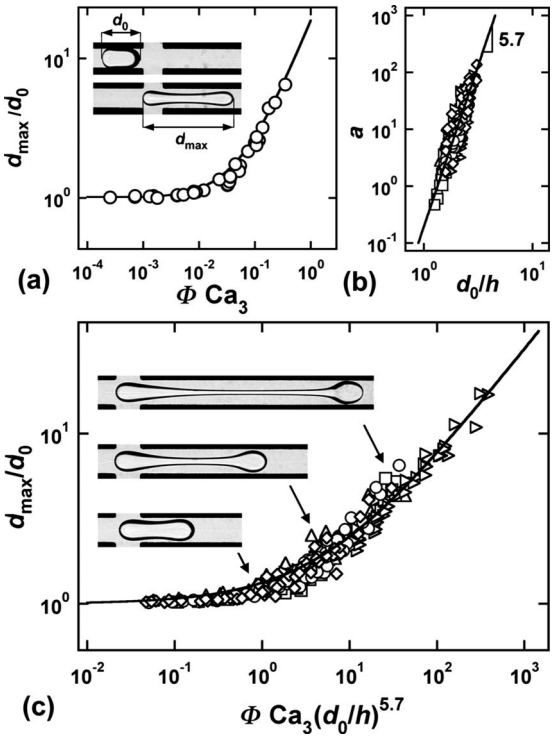

FIG. 4. Maximum droplet elongation in the junction. (a) Dimensionless elongation d_{max}/d_0 vs superficial velocity ratio and cross-flow capillary number ϕCa$_3$ for a fixed initial droplet size $d_0/h=2.0\pm0.1$ and $\chi=85$. Solid line: $d_{max}/d_0=1+a\phi$Ca$_3$, where $a=17.7$. (b) Evolution of prefactor a vs initial droplet size d_0/h for $\chi=17$ (△), 42 (□), 85 (○), 169 (▷), and 426 (◇). Solid line: $a=(d_0/h)^{5.7}$. (c) Evolution of droplet elongation for all fluid pairs and all initial droplet sizes. Solid line: $d_{max}/d_0=1+x^{0.65}$, with $x=\phi$Ca$_3(d_0/h)^{5.7}$.

ness of the lubricating film between the droplet and the walls scales as $\delta\sim$Ca$^{2/3}$ [23], a confined droplet must increase d in order to conserve volume. This morphological change is relatively modest for Ca$<10^{-1}$ and data is well fitted by $d_F/d_0=1+a$Ca^b, with $a=3.6$ and $b=0.74$ [Fig. 3(a), inset]. Although the evolution of d is smooth, V_N and V_R evolve in a rather complex manner [Fig. 3(b)]. Data suggest that translated droplets retract from the rear since V_N first reaches the terminal velocity V_F and $V_R>V_N$ during relaxation. The presence of a thick lubricating film between droplets and walls allows V_F to surpass the homogeneous superficial velocity $J_F=(\Sigma Q_i)/h^2$.

Figure 3(c)-inset displays length evolutions for droplets having similar initial size but different elongations d_{max} for $\chi=85$. The time is normalized by the viscous-capillary time scale $t_c=h\eta_1/\gamma_{12}$ [24]. Remarkably, when d is normalized by d_{max}, relaxation lengths collapse into a nearly linear curve that can be fitted by $d/d_{max}=1+k_1(t/t_c)$ for early time, i.e., $t/t_c\leq 2$ [Fig. 3(c)]. Polynomial functions of time were shown to closely fit the shapes of unbounded relaxing drops numerically computed from Stokes equations for χ ranging between 0.01 and 10 [25]. In these simulations, for $\chi=10$ and large deformations, the first-order coefficient is at least two orders of magnitude larger than higher coefficients, confirming a quasilinear behavior for early times. Here, in the case of

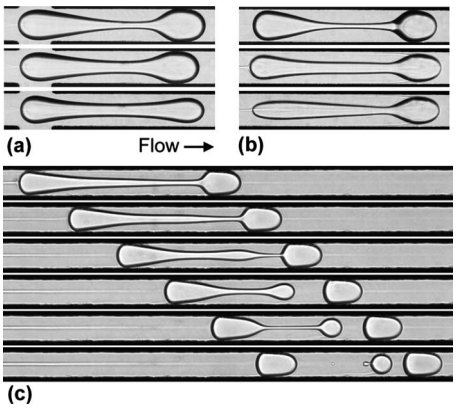

FIG. 5. Spoon-shaped droplets: morphology during convective breakup. (a) Influence of Ca on droplet symmetry and confinement at the channel junction ($h=250$ μm and $\chi=85$), from top to bottom: Ca$=5\times10^{-3}$, 8×10^{-3}, and 2×10^{-2}. (b) Spoon-shaped droplets in straight square microchannel ($h=250$ μm), from top to bottom: "tea spoon" ($\chi=83$), "dessert spoon" ($\chi=17$), and "salad spoon" ($\chi=17$). (c) Time series of a complex fragmentation process $\Delta t=10$ ms ($h=100$ μm and $\chi=42$).

strongly confined droplets, k_1 is measured for χ ranging between 17 and 426 and we find $k_1=-0.068$ relatively independent of χ [Fig. 3(d)]. Uncertainty arises in k_1, in part, due to droplet relaxation in the direction normal to the flow, and the influence of the translation velocity. Over the range of parameters investigated, since the variability of k_1 is negligible compared to the 25-fold change of t_c, the relationship $d/d_{max}=1+k_1(t/t_c)$ is useful for predicting relaxation processes. These results show that microfluidic droplets elongated in threads initially recoil at a nearly constant velocity, which is inversely proportional to the droplet viscosity η_1.

The maximal elongation d_{max} is an important feature that can be determined using a scaling analysis. Comparing the "feeding" time in the junction $t_0\approx d_0/V_0$ with the typical stretching or "ingesting" time $t_f\approx d_{max}/V_F$ yields $d_{max}/d_0\propto\phi$ where $\phi=V_F/V_0$ is the velocity ratio. However, since viscous stresses tend to deform drops while interfacial tension stresses tend to resist deformation, d_{max}/d_0 should also scale with the side-flow capillary number Ca$_3$. Combining these two arguments yields $d_{max}/d_0\propto\phi$Ca$_3$. We compare experimental d_{max} with this parameter for a fixed initial size $d_0/h=2.0\pm0.1$, and find the following fit: $d_{max}/d_0=1+a\phi$Ca$_3$, with $a=17.7$ [Fig. 4(a)]. A relatively small deviation in d_0, however, introduces significant scatter, suggesting that the factor a is also a function of d_0. Therefore, $a=(d_{max}/d_0-1)/(\phi$Ca$_3)$ is plotted versus d_0/h and we find $a\approx(d_0/h)^{5.7}$ [Fig. 4(b)]. For both relaxing and convective breakup regimes, this scaling is used to empirically determine the dimensionless parameter ϕCa$_3(d_0/h)^{5.7}$ that allows for collapsing d_{max}/d_0 into a master curve with χ ranging between 17 and 426 [Fig. 4(c)]. The large exponent is consistent with the fact that a large range of deformations occurs for a small range of d_0/h that spans between 1 and 3.

During deformation, droplets display a variety of time-dependent morphology as a function of flow and fluid parameters [Fig. 5]. Previous studies using four-roll mill extensional flows have shown that as Ca increases, droplets

typically deform into a symmetric slender thread characterized by pointed ends for $\chi \ll 1$ and by a dumbbell shape with two bulbous ends for $\chi \sim 1$ [2]. Here, a similar behavior is observed as elongated droplet ends become more rounded when χ increases from 17 to 426. Due to the relative importance of the microfluidic confinement and pressurized flow, the dumbbell shape is asymmetric for low Ca since droplets are more sensitive to pressure variations in the capillary regime. As Ca increases, viscous stresses dominate capillary stresses, and the shape becomes more symmetrical and confined by the external fluid at the walls [Fig. 5(a)]. Asymmetrical droplets display morphologies that resemble "spoons" [Fig. 5(b)]. Similar to end-pinching fragmentation in a quiescent unbounded fluid [26–30], a translating droplet can undergo multiple breakups leading to a variety of satellite droplets [Fig. 5(c)]. We observe, however, that the front droplet splits first from the overall structure. This type of complex fragmentation process is also observed in the absolute breakup regime.

This study shows that microfluidic confinement strongly influences droplet deformation by introducing specific length scales. Similar to unbounded flows [31], the initial drop shape is shown to play a major role in subsequent droplet deformation and breakup. In the asymptotic regime associated with large χ, our results suggest that confined relaxation is dominated by the viscosity of the droplet η_1 while confined stretching is relatively independent from η_1. Further investigations should elucidate the influence of the continuous phase viscosity η_2 and the asymmetry in the fine structure of translated droplets. Such a two-step hydrodynamic focusing design, which was previously used to investigate complex dispersions such as miscible swirls [32] and double emulsions [33], is particularly promising for performing multistep microreactions using viscous materials. Overall, the use of large velocity contrasts between streams at microchannel junctions is an effective tool for altering the morphology of capillary objects.

[1] J. M. Rallison, Annu. Rev. Fluid Mech. **16**, 45 (1984).
[2] H. A. Stone, Annu. Rev. Fluid Mech. **26**, 65 (1994).
[3] L. G. Leal, Phys. Fluids **16**, 1833 (2004).
[4] H. A. Stone, B. J. Bentley, and L. G. Leal, J. Fluid Mech. **173**, 131 (1986).
[5] W. L. Olbricht, Annu. Rev. Fluid Mech. **28**, 187 (1996).
[6] A. Borhan and J. Pallinti, Phys. Fluids **11**, 2846 (1999).
[7] T. M. Squires and S. R. Quake, Rev. Mod. Phys. **77**, 977 (2005).
[8] S. Y. Teh, R. Lin, L. H. Hung, and A. P. Lee, Lab Chip **8**, 198 (2008).
[9] P. Garstecki, M. Fuerstman, H. A. Stone, and G. W. Whitesides, Lab Chip **6**, 437 (2006).
[10] G. F. Christopher and S. L. Anna, J. Phys. D **40**, R319 (2007).
[11] T. Cubaud and T. G. Mason, Phys. Fluids **20**, 053302 (2008).
[12] D. R. Link, S. L. Anna, D. A. Weitz, and H. A. Stone, Phys. Rev. Lett. **92**, 054503 (2004).
[13] L. Ménétrier-Deremble and P. Tabeling, Phys. Rev. E **74**, 035303(R) (2006).
[14] L. Prat, F. Sarrazin, J. Tasseli, and A. Marty, Microfluid. Nanofluid. **2**, 271 (2006).
[15] A. M. Leshansky and L. M. Pismen, Phys. Fluids **21**, 023303 (2009).
[16] T.-M. Tsai and M. J. Miksis, J. Fluid Mech. **274**, 197 (1994).
[17] D. J. E. Harvie, M. R. Davidson, J. J. Cooper-White, and M. Rudman, Chem. Eng. Sci. **61**, 5149 (2006).
[18] Y. C. Tan, Y. L. Ho, and A. P. Lee, Microfluid. Nanofluid. **3**, 495 (2007).
[19] N. Bremond, A. R. Thiam, and J. Bibette, Phys. Rev. Lett. **100**, 024501 (2008).
[20] H. Boukellal, S. Selimovic, Y. Jia, C. G., and S. Fraden, Lab Chip **9**, 331 (2009).
[21] N. Rashidnia, R. Balasubramaniam, and D. Del Signore, AIChE J. **38**, 615 (1992).
[22] B. Ambravaneswaran, H. J. Subramani, S. D. Phillips, and O. A. Basaran, Phys. Rev. Lett. **93**, 034501 (2004).
[23] J. Ratulowski and H.-C. Chang, Phys. Fluids A **1**, 1642 (1989).
[24] J. Eggers, Rev. Mod. Phys. **69**, 865 (1997).
[25] M. Tjahjadi, J. M. Ottino, and H. A. Stone, AIChE J. **40**, 385 (1994).
[26] J.-W. Ha and L. G. Leal, Phys. Fluids **13**, 1568 (2001).
[27] P. K. Notz and O. A. Basaran, J. Fluid Mech. **512**, 223 (2004).
[28] A. Y. Tong and Z. Wang, Phys. Fluids **19**, 092101 (2007).
[29] R. M. S. M. Schulkes, J. Fluid Mech. **309**, 277 (1996).
[30] P. K. Notz, A. U. Chen, and O. A. Basaran, Phys. Fluids **13**, 549 (2001).
[31] H. A. Stone and L. G. Leal, J. Fluid Mech. **206**, 223 (1989).
[32] T. Cubaud and T. G. Mason, Phys. Rev. Lett. **98**, 264501 (2007).
[33] N. Pannacci, H. Bruss, D. Bartolo, I. Etchart, T. Lockhart, Y. Hennequin, H. Willaime, and P. Tabeling, Phys. Rev. Lett. **101**, 164502 (2008).